




# Mitoribosomal small subunit maturation involves formation of initiation-like complexes

Tea Lenarčić<sup>a,1</sup>, Moritz Niemann<sup>b,1,2</sup>, David J. F. Ramrath<sup>a</sup>, Salvatore Calderaro<sup>b</sup>, Timo Flügel<sup>a</sup>, Martin Saurer<sup>a</sup>, Marc Leibundgut<sup>a</sup>, Daniel Boehringer<sup>a,3</sup>, Céline Prange<sup>a</sup>, Elke K. Horn<sup>b</sup>, André Schneider<sup>b,4</sup> , and Nenad Ban<sup>a,4</sup>

<sup>a</sup>Department of Biology, Institute of Molecular Biology and Biophysics, ETH Zurich, CH-8093 Zurich, Switzerland; and <sup>b</sup>Department of Chemistry, Biochemistry, and Pharmaceutical Sciences, University of Bern, CH-3012 Bern, Switzerland

This contribution is part of the special series of Inaugural Articles by members of the National Academy of Sciences elected in 2021.

Contributed by Nenad Ban; received August 16, 2021; accepted October 29, 2021; reviewed by Sebastian Klinge and John Woolford

**Mitochondrial ribosomes (mitoribosomes) play a central role in synthesizing mitochondrial inner membrane proteins responsible for oxidative phosphorylation. Although mitoribosomes from different organisms exhibit considerable structural variations, recent insights into mitoribosome assembly suggest that mitoribosome maturation follows common principles and involves a number of conserved assembly factors. To investigate the steps involved in the assembly of the mitoribosomal small subunit (mt-SSU) we determined the cryoelectron microscopy structures of middle and late assembly intermediates of the *Trypanosoma brucei* mitochondrial small subunit (mt-SSU) at 3.6- and 3.7-Å resolution, respectively. We identified five additional assembly factors that together with the mitochondrial initiation factor 2 (mt-IF-2) specifically interact with functionally important regions of the rRNA, including the decoding center, thereby preventing premature mRNA or large subunit binding. Structural comparison of assembly intermediates with mature mt-SSU combined with RNAi experiments suggests a noncanonical role of mt-IF-2 and a stepwise assembly process, where modular exchange of ribosomal proteins and assembly factors together with mt-IF-2 ensure proper 9S rRNA folding and protein maturation during the final steps of assembly.**

structural biology | translation | mitochondria | ribosome assembly

**D**uring translation, proteins are synthesized by ribosomes, large ribonucleoprotein complexes present in the cytoplasm of bacterial and eukaryotic cells (1). Ribosomes are also found in cell organelles of bacterial ancestry, such as mitochondria (2) and chloroplasts (3). Although bacterial and mitochondrial ribosomes (mitoribosomes) share a common ancestor, structures of mitoribosomes revealed extensive evolutionary changes in terms of composition and structure (4–8). Furthermore, mitoribosomes acquired many other unique functional features, such as a customized exit tunnel, since they are highly specialized for the synthesis of essential components of respiratory complexes located in the mitochondrial membranes (9–13).

Due to their complexity, ribosome assembly requires participation of many assembly factors and processing enzymes that facilitate folding, compaction, and covalent modifications of the rRNA and sequential association of the ribosomal proteins to yield properly assembled and translationally active particles (14). Thus far, many bacterial and eukaryotic ribosomal intermediates have been biochemically and structurally characterized, providing important mechanistic insights into ribosome assembly (15–17). Bacterial ribosomes can be reconstituted *in vitro* from free rRNA and ribosomal proteins through thermodynamically interdependent protein-binding steps (18, 19); however, *in vivo* the biogenesis process involves a few dozens of assembly factors (15). Eukaryotic ribosome assembly is much more complex due to cell compartmentalization (20) and is consequently mediated by over 200 ribosome assembly factors and small nucleolar RNAs (21). Additionally, components of the cytosolic translation machinery were reported to assist in the late stages of ribosome assembly by checking the quality of functionally important sites

in the ribosome (22). Interestingly, it was reported for bacteria that at low temperatures a cold-sensitive initiation factor 2 (IF-2) mutation causes the accumulation of immature ribosomal particles, suggesting a participation of IF-2 in ribosome assembly (23).

Despite an increasing number of identified mitoribosomal assembly factors (24), the knowledge about the molecular details of ribosome assembly in mitochondria remains limited. Additional difficulties in studying mitoribosome assembly stem from the fact that nearly all mitoribosomal proteins are encoded by nuclear genes, translated on cytoplasmic ribosomes, and imported into mitochondria, where they associate with mitochondrial rRNA. Recent results suggest that in human initial interaction of mitoribosomal proteins and rRNA commences at the mitochondrial nucleoprotein compartments, the nucleoids (25). Upon early small subunit (SSU) and large subunit (LSU) assembly, intermediates relocate to another mitochondrial compartment adjacent to inner membranes, the RNA granules, where mitoribosome assembly concludes (26). Understanding how these large and complex cellular machineries assemble in mitochondria and

## Significance

**Mitochondria originated from ancestral bacteria and they still maintain their own reduced genome and translational apparatus that feature highly diverged mitoribosomes, specialized for the synthesis of membrane proteins. Only recently, high-resolution cryo-EM structures of the mature mitoribosomes from several species revealed their unusual structural features. Nevertheless, the mechanisms of their assembly are relatively poorly understood. To better understand how mitoribosomes are assembled and which factors participate in this process, we investigated assembly intermediates of the small mitoribosomal subunit from *Trypanosoma brucei* to reveal that the process involves a modular stepwise exchange of assembly factors that facilitate the formation of the functional decoding center of the small ribosomal subunit, and we discovered that mitochondrial initiation factor 2 participates in this process.**

Author contributions: T.L., M.N., D.J.F.R., A.S., and N.B. designed research; T.L., M.N., D.J.F.R., S.C., T.F., C.P., and E.K.H. performed research; T.L., M.N., D.J.F.R., S.C., T.F., M.S., M.L., D.B., C.P., A.S., and N.B. analyzed data; and T.L., M.N., A.S., and N.B. wrote the paper.

Reviewers: S.K., Rockefeller University; and J.W., Carnegie Mellon University.

The authors declare no competing interest.

This open access article is distributed under [Creative Commons Attribution-NonCommercial-NoDerivatives License 4.0 \(CC BY-NC-ND\)](https://creativecommons.org/licenses/by-nc-nd/4.0/).

<sup>1</sup>T.L. and M.N. contributed equally to this work.

<sup>2</sup>Present address: Mattei team, EMBL Imaging Centre, 69117 Heidelberg, Germany.

<sup>3</sup>Present address: Cryo-EM Knowledge Hub, ETH Zurich, CH-8093 Zurich, Switzerland.

<sup>4</sup>To whom correspondence may be addressed. Email: andre.schneider@dcb.unibe.ch or ban@mol.biol.ethz.ch.

This article contains supporting information online at <http://www.pnas.org/lookup/suppl/doi:10.1073/pnas.2114710118/-DCSupplemental>.

Published January 18, 2022.

how the import of ribosomal proteins from the cytoplasm is coordinated with the transcription of the rRNA within the mitochondrion is also relevant for biomedical research. Mutations of mitoribosomal proteins or rRNA cause impaired assembly of mitoribosomal subunits that lead to several disorders, such as Leigh syndrome, sensorineural hearing loss, encephalomyopathy, hypertrophic cardiomyopathy (27–29), and cancer (30).

Recently, first mechanistic insights into the assembly of mitoribosomes were obtained by structure determinations of the kinetoplastid small (mt-SSU) (31, 32) and large subunit (mt-LSU) (32–34) as well as late-stage human mt-LSU assembly intermediates (35–40). The study of untagged *Trypanosoma brucei* mt-SSU resulted in several cryogenic electron microscopy (cryo-EM) structures of assembly intermediates that illustrated possible assembly progression. However, only the mt-SSU assemblosome, the earliest and the most prominent, could be interpreted at atomic resolution, revealing an elaborate assembly machinery consisting of 34 small ribosomal subunit assembly factors (mt-SAFs) (31). To better understand the individual steps of mitoribosome assembly, we determined the molecular structures of the two intermediates that were identified in that study. Both assembly intermediates reveal a more mature 9S rRNA compared to the mt-SSU assemblosome and participation of five additional mt-SAFs as well as mitochondrial initiation factor 2 (mt-IF-2) in the assembly process. Structural analysis of the complexes shows that the mt-IF-2 N-terminal domain (NTD), together with a mitochondrial initiation factor 3 (mt-IF-3)-like assembly factor mt-SAF39, contact the functionally important decoding center to monitor its proper fold and block the mRNA channel, thereby likely preventing premature mRNA binding or subunit joining. Our structural and biochemical results provide key insights into the late-stage steps of trypanosomal mitoribosome maturation and reveal that the assembly involves formation of initiation-like complexes.

## Results

**Cryo-EM Structures of Middle and Late Small Subunit Assembly Intermediates.** The observation that the mt-SSU middle and late assembly intermediates were found in the cryo-EM dataset of the native mitochondrial sample from *T. brucei* (31) prompted us to search all previously obtained cryo-EM datasets that were prepared for investigations of the mature mt-SSU, mt-LSU, and a nearly complete mitoribosome (7) for the presence of mt-SSU assembly intermediates using the available low-resolution maps of the intermediates as references (31). We found classes representing mt-SSU assembly intermediates in all datasets, independent of whether the native or tag-assisted purification of mitoribosomes was performed. We were able to calculate a cryo-EM map of the middle assembly intermediate at 3.6-Å resolution by reprocessing of the cryo-EM dataset containing SSU-tagged mitoribosomes (Fig. 1A and *SI Appendix, Figs. S1 and S2 and Table S1*). Particles representing the late assembly intermediate were found in the SSU- and LSU-tagged mitoribosome cryo-EM datasets. Merging the particles from both datasets allowed us to reconstruct a late assembly intermediate map at 3.7-Å resolution (Fig. 1A and *SI Appendix, Figs. S3 and S4*).

Middle and late assembly intermediates lack the mt-SSU assemblosome-specific wedge between the mt-SSU head and body and therefore in overall appearance resemble more the mature mt-SSU but vary in the 9S rRNA maturation level as well as in the number of mt-SSU ribosomal proteins and mt-SAFs (Fig. 1B and C). Although not as extensive as the assembly machinery in mt-SSU assemblosome, the middle assembly intermediate comprises 20 nonribosomal proteins in total (Fig. 1B). Among these, 15 were previously identified as mt-SAFs in the mt-SSU assemblosome and, during conversion

from the middle to the late assembly intermediate, 10 of these assembly factors dissociate, whereas 5 of them persist across both intermediates (Fig. 1B and C). In addition to these, we identified in both complexes five previously undescribed nonribosomal proteins that we assigned as middle and late assembly intermediate-specific small subunit assembly factors, namely mt-SAF35, mt-SAF36, mt-SAF37, mt-SAF38, and mt-SAF39 (*SI Appendix, Fig. S5 and Table S2*). Some show structural homology to known enzymes, such as FAD-dependent DNA photolyase (mt-SAF35) (41), malonyl-CoA-acyl carrier protein transferase (mt-SAF36) (42), and a double hot dog thioesterase/dehydratase fold (mt-SAF38) (43, 44) (*SI Appendix, Fig. S6*). Along with the group of the additional mt-SAFs, we discovered that mitochondrial initiation factor 2 (mt-IF-2) is a tightly interacting component of both assembly intermediates (Fig. 1 and *SI Appendix, Table S2*). To ascertain the functional role of these mt-SAFs in the assembly process, we used RNA interference (RNAi) knockdown experiments and in all cases observed growth retardation and a decrease of the mt-SSU 9S rRNA stability (Fig. 2). Like mt-LAF3 in the mt-LSU assembly (33), RNAi-mediated gene knockdown of the malonyl-CoA-acyl carrier protein transferase homolog mt-SAF36 (*SI Appendix, Fig. S6*) affects the stability of both the mt-SSU 9S and the mt-LSU 12S rRNA (Fig. 2). This suggests that mt-SAF36 plays an additional role in LSU maturation directly or indirectly via disturbing a mitochondrial process such as fatty acid metabolism, which upon mt-SAF36 knockdown might generally impair mitochondria and eventually lead to mitoribosome disintegration.

Major differences between the two intermediates are also reflected in their mitoribosomal protein content. The middle assembly intermediate lacks 8 mitoribosomal proteins out of 55, whereas the late assembly intermediate carries the full set of proteins present in the mature mt-SSU. The observation that the late assembly intermediate contains a complete set of mitoribosomal proteins, almost fully matured 9S rRNA and a smaller number of assembly factors compared to the middle intermediate (Fig. 1) is in agreement with our previous assumptions regarding the sequential order of assembly (31).

**Molecular Composition of Assembly Intermediates Implies a Stepwise Assembly.** By comparing the structures of the middle and late assembly intermediates, we observed a large-scale exchange of proteins between the two complexes (Fig. 3). Mt-SAFs that are preserved from the mt-SSU assemblosome, in particular mt-SAF2 (KRIPP2), mt-SAF5, mt-SAF21, mt-SAF23, mt-SAF26, mt-SAF27, mt-SAF29, mt-SAF31, mt-SAF32, and mt-SAF33, cover the solvent-exposed side in the middle assembly intermediate and consequently prevent the binding of mitoribosomal proteins that constitute a large portion of the mature mt-SSU body (Fig. 3A). In the late assembly intermediate, however, they are replaced by mitoribosomal proteins mS42, mS43, mS47, mS48, mS60, mS61, mS64, and mS66. This allows the solvent-exposed side to fully mature, indicating an important turning point between middle and late assembly intermediates (Fig. 3B). Concomitantly, several mitoribosomal proteins at the solvent-exposed side undergo structural changes to assume mature mt-SSU conformation. Although the group of assembly factors seems to be directly exchanged by a cluster of ribosomal proteins that bind to the same location on the immature mt-SSU, none of them with the exception of mt-SAF33 exhibits sequence or structural homology to mitoribosomal proteins (Fig. 3).

Despite complete maturation at the solvent-exposed side in the late assembly intermediate, functionally important regions of the intersubunit sides in both complexes remain shielded by five mt-SAFs specific for the middle and late assembly intermediates (mt-SAF35–39), five mt-SAFs that are in common with the

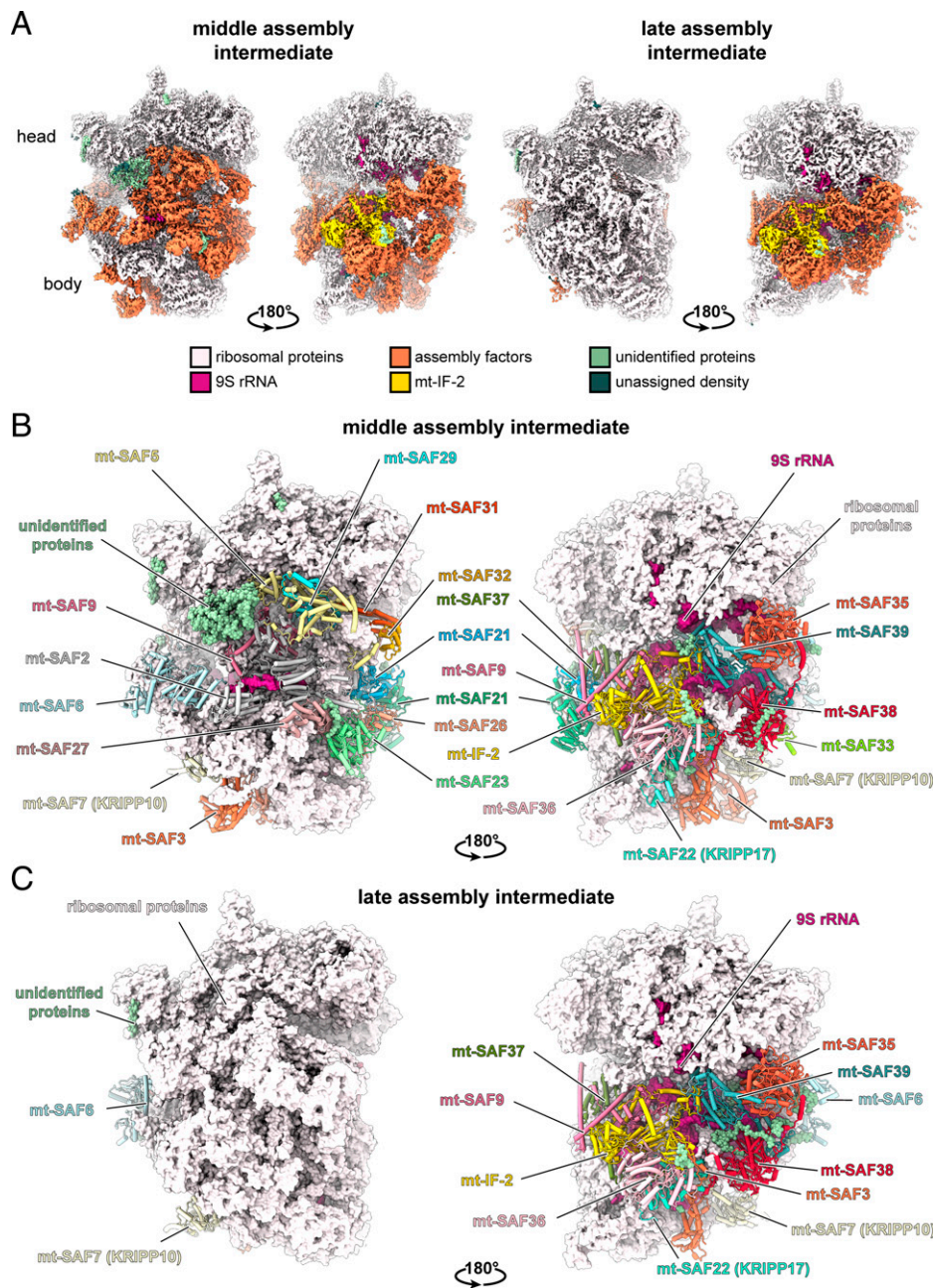


**Fig. 1.** Architectural overview of the *T. brucei* middle and late mt-SSU assembly intermediates. (A) The cryo-EM reconstructions show density and atomic models of the middle (B) and late (C) assembly intermediates.

mt-SSU assemblosome (mt-SAF3, mt-SAF6, KRIPP10, mt-SAF9, and KRIPP17), and, importantly, the mt-IF-2 (Fig. 3). Such an intersubunit-side shielding strategy is common in the ribosomal maturation process, as several structures of bacterial as well as cytosolic intermediates of the ribosomal small subunit revealed that late-stage assembly factors localize near the decoding site in order to conformationally proofread this region and to prevent premature translation initiation (45–48).

**Assembly Factors Control mt-SSU rRNA Maturation.** Compared to the mature 9S rRNA, the 9S rRNAs of middle and late assembly intermediates adopt an immature conformation in several regions across the structure, with the 9S rRNA of the middle assembly intermediate being significantly less mature than the one of the late assembly intermediate (Fig. 4A and *SI Appendix, Fig. S7A*).

Whereas the majority of the 5' and 3' major domains resemble the mature 9S rRNA conformation, large parts of the central and 3' minor domains in the 9S rRNA of the middle assembly intermediate appear to be more dynamic and cannot be interpreted at atomic detail (Fig. 4A and *SI Appendix, Fig. S7B*). The immature regions of the 9S rRNA in the middle assembly intermediate are stabilized through extensive interactions with several mt-SAFs (Fig. 4B). As in the mt-SSU assemblosome, the 9S rRNA 5' end of the middle assembly intermediate remains extended due to extensive interactions with mt-SAF2 (KRIPP2). The absence of mt-SAF2 in the late assembly intermediate enables the 9S rRNA 5' end to contract and interact with mitoribosomal proteins. Moreover, in the mt-SSU assemblosome the immature h22/h23 region is bound to mt-SAF7 (KRIPP10), mt-SAF18, mt-SAF28, mt-SAF30, and mt-SAF33. All factors except mt-SAF7 and

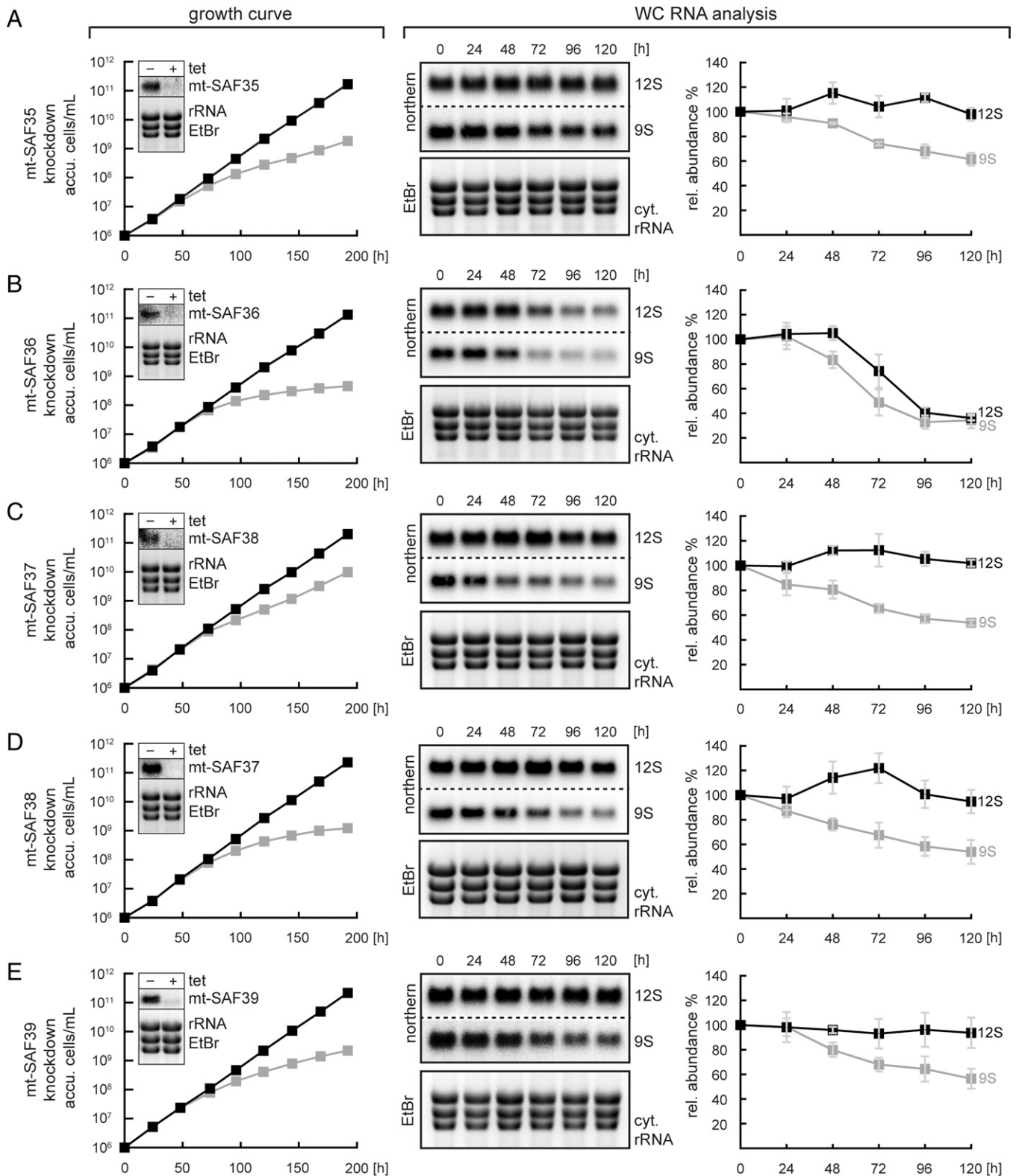


**Fig. 2.** Significance of assembly factors for cell growth and rRNA stability. (A–E) The protein levels of assembly factors mt-SAF35–39 of the middle and late assembly intermediates were reduced by tetracycline (tet)-inducible RNAi in *T. brucei* cells. All cultures started showing reduced growth 72 h after induction of the assembly factor knockdowns: black squares, no tet; gray squares, plus tet. The *Inset* contains the mRNA Northern blot showing the ablation of the corresponding assembly factor mRNA, and the ethidium bromide (EtBr) stain of cytosolic rRNA serves as a loading control. The levels of 12S and 9S rRNA in the knockdown strains were followed in 24-h intervals by Northern blotting. The cytosolic (cyt) rRNAs stained by EtBr are shown as loading control. Cultures were grown in triplicates. In all panels, error bars indicate the average deviation from the mean.

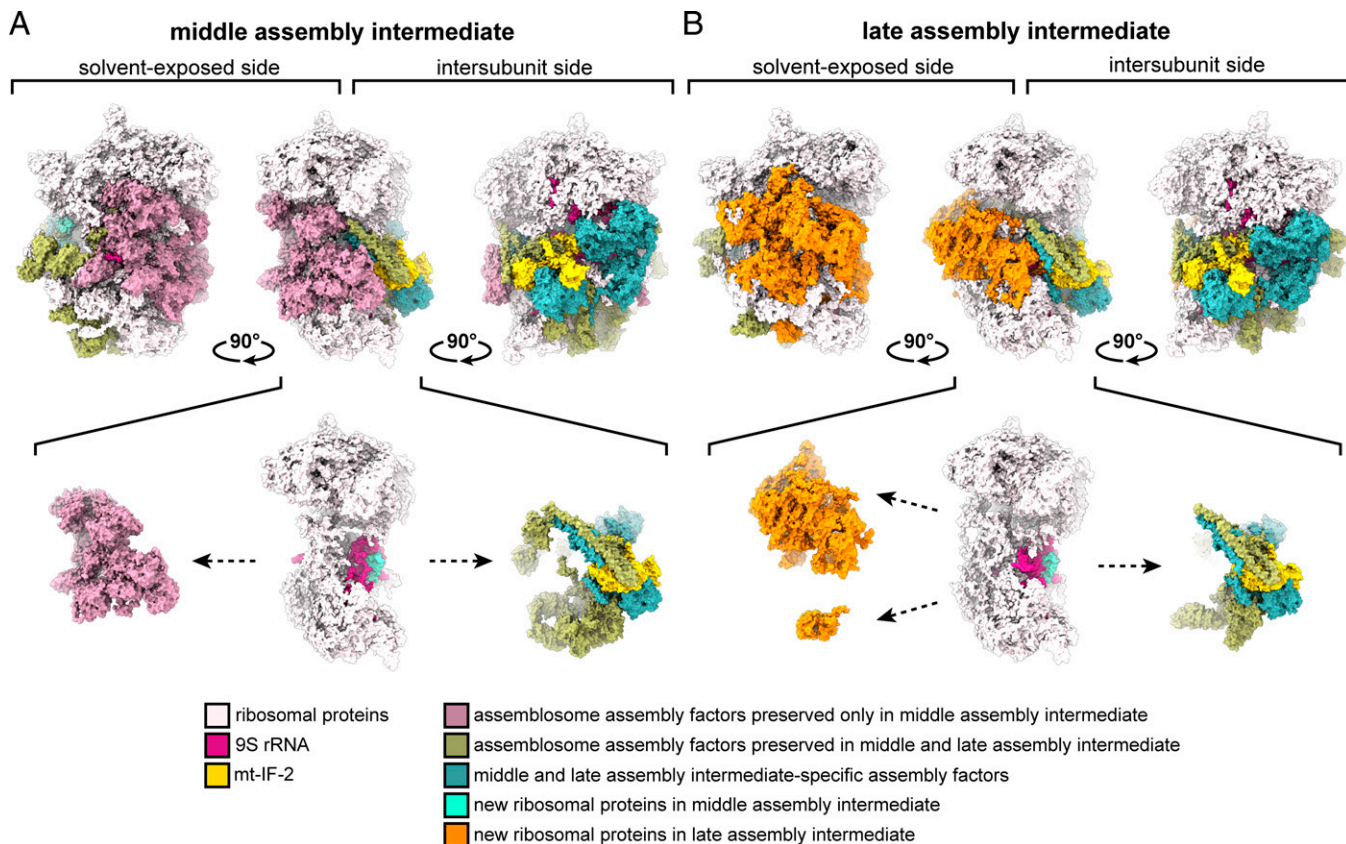


**Fig. 3.** Molecular composition comparison between middle (A) and late (B) assembly intermediates. Ribosomal proteins and assembly factors are colored depending on the stage at which they are associated with the mt-SSU.

mt-SAF33 are replaced by the middle and late intermediate-specific mt-SAF38 and mt-SAF39, an exchange that opens up space allowing helix h23 to rotate and extend. The final transformation to the mature and extended conformation of helices h22 and h23 occurs when two mitoribosomal proteins, bS21m and mS37, assume their native conformation in the late assembly intermediate and form a structural platform on which the 9S rRNA is remodeled. The only part of the 9S rRNA that remains in a substantially immature conformation in the late assembly intermediate is the functionally important helix h44 adjacent to the decoding center (Fig. 4A and *SI Appendix*, Fig. S7B). In the mt-SSU assembly, the immature h44 is stabilized by mt-SAF11, mt-SAF14, mt-SAF18, mt-SAF22 (KRIPP17), and mt-SAF24 (Fig. 4B). Partial rearrangement of the base-pairing pattern and contraction of the helix take place upon dissociation of mt-SAF11, mt-SAF14, mt-SAF18, and mt-SAF24, and the association of the assembly factors mt-SAF36, mt-SAF39, and mt-IF-2, as well as the remodeling of mt-SAF3. For h44 to mature completely, a structural rearrangement of mS38 has to occur, and all assembly factors have to dissociate.

**Mitochondrial Initiation Factor 2 and an Initiation Factor 3-Like Assembly Factor Play a Role in the Maturation of the Decoding Center.** In both assembly intermediates, the decoding center possesses all crucial elements for translation, such as ribosomal protein uS12m, 9S rRNA h18, and nearly mature h44. At this stage, also the mRNA channel is formed (Fig. 5A). However, mt-IF-2 and mt-IF3-like mt-SAF39 constitute a large portion of the proteinaceous shield that covers the decoding center on the intersubunit side (Fig. 5B). They form extensive interactions with the 9S rRNA in regions h16-18, h23, and h44 (Fig. 5C).

The presence of mt-IF-2 in the assembly intermediates is interesting, since it was not only identified as a bona fide initiation factor based on sequence homology but was also shown to participate in translation initiation based on biochemical experiments, which revealed that *T. brucei* mt-IF-2 selectively binds formylated trypanosomal elongator tRNA(Met) that acts as mitochondrial initiator tRNA(Met) in trypanosomes (49, 50). In the late assembly intermediate, almost the entire mt-IF-2 is well resolved, revealing a similar domain organization as in mammalian mt-IF-2 with an NTD, G domain, domains II, III, and IV, and a linker between domains II and III (Fig. 5D).

The G domain of trypanosomal mt-IF-2 is highly conserved (*SI Appendix*, Fig. S8A) and includes a GTP binding site that together with the switch loops faces toward the adjacent mt-SAF36, while the catalytic histidine H261, which is crucial for GTP hydrolysis, adopts an inactive conformation (*SI Appendix*, Fig. S8B and C). Accordingly, we observe a GDP with a partially occupied inorganic phosphate bound to the G domain (*SI Appendix*, Fig. S8B and C). From the other side, the G domain is locked in place by mt-SAF9 (*SI Appendix*, Fig. S8B). Interestingly, the two assembly factors occupy similar positions as mt-LSU bL12m and the sarcin/ricin loop found in the active conformation of the mammalian mitochondrial translation initiation complex (12) (*SI Appendix*, Fig. S8B). While mt-LSU binding induces GTP hydrolysis that causes long-range conformational changes in domain IV of mt-IF-2, resulting in the release and an insertion of the initiator tRNA into the P site (12), a similar hydrolysis event followed by a conformational change triggered by mt-SAF9 and mt-SAF36 might play a role during mitoribosomal maturation. Further emphasizing a noncanonical configuration of the mt-IF-2 in the assembly

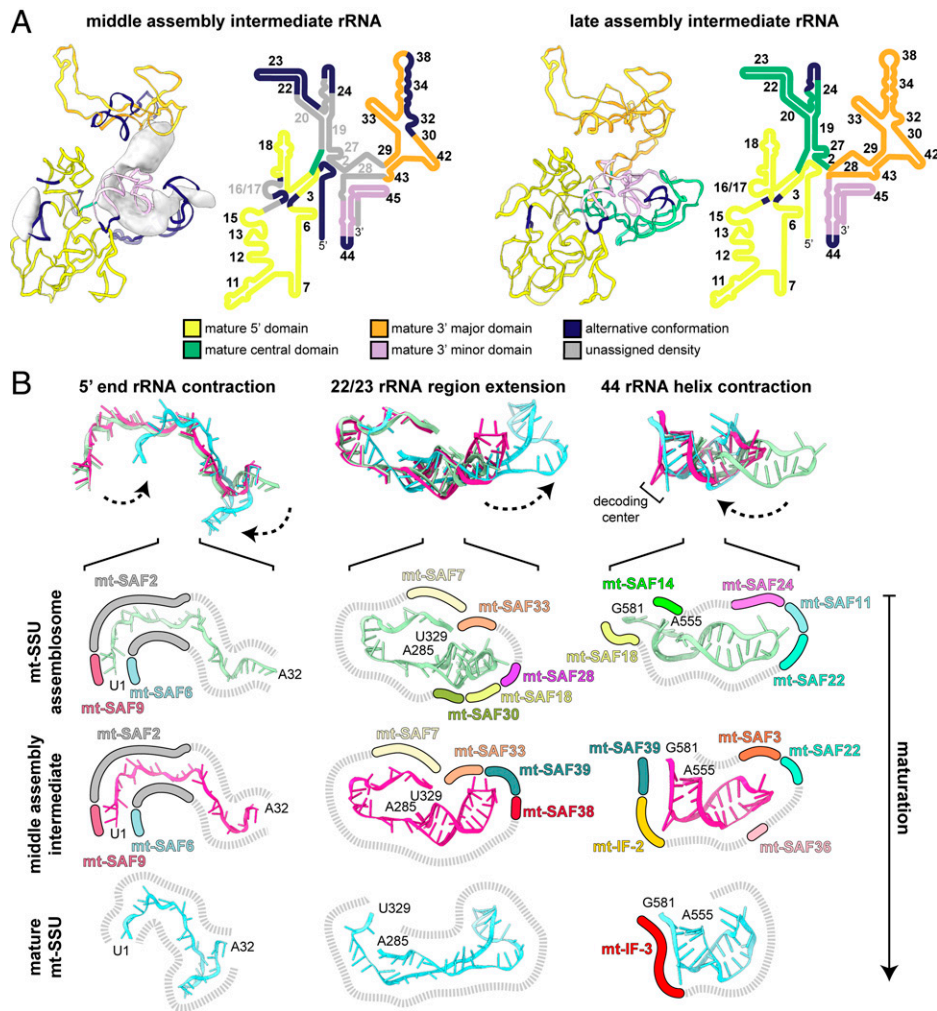


**Fig. 4.** Maturation process of the *T. brucei* 9S rRNA. (A) Three-dimensional structures of the middle (Left) and late (Right) assembly intermediate 9S rRNAs with corresponding secondary structure diagram from the intersubunit side. The 9S rRNA regions are labeled according to their conformational state. A low-pass filtered density represents regions of rRNA in the middle assembly intermediate that were not sufficiently resolved for atomic model building (depicted gray in the diagram). (B) Conformational changes of the 9S rRNA 5' end, the h22/h23 region and h44 that occur during maturation from the mt-SSU assemblosome through the middle assembly intermediate to the mature mt-SSU are depicted with dashed arrows. 9S rRNA maturation is steadily aided by a number of assembly factors and mt-IF-2, all of which are highlighted schematically and colored individually.

process, we do not find any density in the map that would correspond to tRNA bound to the ternary complex. Instead, the tRNA binding pocket of domain IV in mt-IF-2 is occupied by an unidentified protein density, possibly serving to block a premature formation of the ternary complex. In addition, trypanosomal mt-IF-2 domain IV is held in place by a contact with a conserved loop of mt-SAF36, resulting in an outward rotation that would not be compatible with correct positioning of the tRNA in the decoding site, as observed for the tRNA-bound mammalian mt-IF-2 during initiation (Fig. 5D) (12). Notably, compared to its mammalian counterpart, the linker between domains II and III in trypanosomal mt-IF-2 is shorter and lacks the specific insertion that structurally and functionally substitutes for bacterial IF-1 in mammalian mitochondrial translation initiation (12). This is in line with our previous observation that, in *T. brucei*, the functional role of bacterial IF-1 (51) is likely taken over by mt-IF-3 (7).

In addition to the participation of mt-IF-2 in mt-SSU assembly, structural comparison of the middle and late assembly intermediate complexes and mature mt-SSU shows that mt-SAF39 occupies a similar position as mt-IF-3 in the mature mt-SSU

(7, 32), and that this factor contains an mt-IF-3-like domain (Fig. 5E) despite sharing low sequence identity (21.2%). Compared to mt-IF-3, mt-SAF39 contains longer N- (NTE) and C-terminal extensions (CTE) (Fig. 5E). The mt-SAF39 CTE stretches into the junction between the mt-SSU head and the body and along with the mt-IF-2 NTD specifically interacts with the 9S rRNA decoding center (Fig. 5F and SI Appendix, Fig. S9). The side chain of Met671 from mt-SAF39 extends in between the flipped-out decoding bases of A576 and A577 (A1542 and A1543 in *Escherichia coli*), whereas the mt-IF-2 NTD, in particular Arg111 and Ser112 from mt-IF-2, splay open helix h44 and as a result additionally stabilize the flipped-out conformations of A576 and A577 (Fig. 5F). Such conformation of the decoding center differs from the mt-IF-3 stabilized conformation of the mature mt-SSU in *T. brucei*, where residues Lys341 and Arg343 promote stacking of the A577 between nucleotides A558 and C578 and a partial flipping-out of A576 (Fig. 5G). Additionally, the mt-SAF39 CTE forms a series of  $\alpha$ -helices (Fig. 5E) that, based on the comparison with the mRNA-containing mammalian mitochondrial ribosome initiation complex (12), partially occupy and occlude the mRNA channel (Fig. 5H).

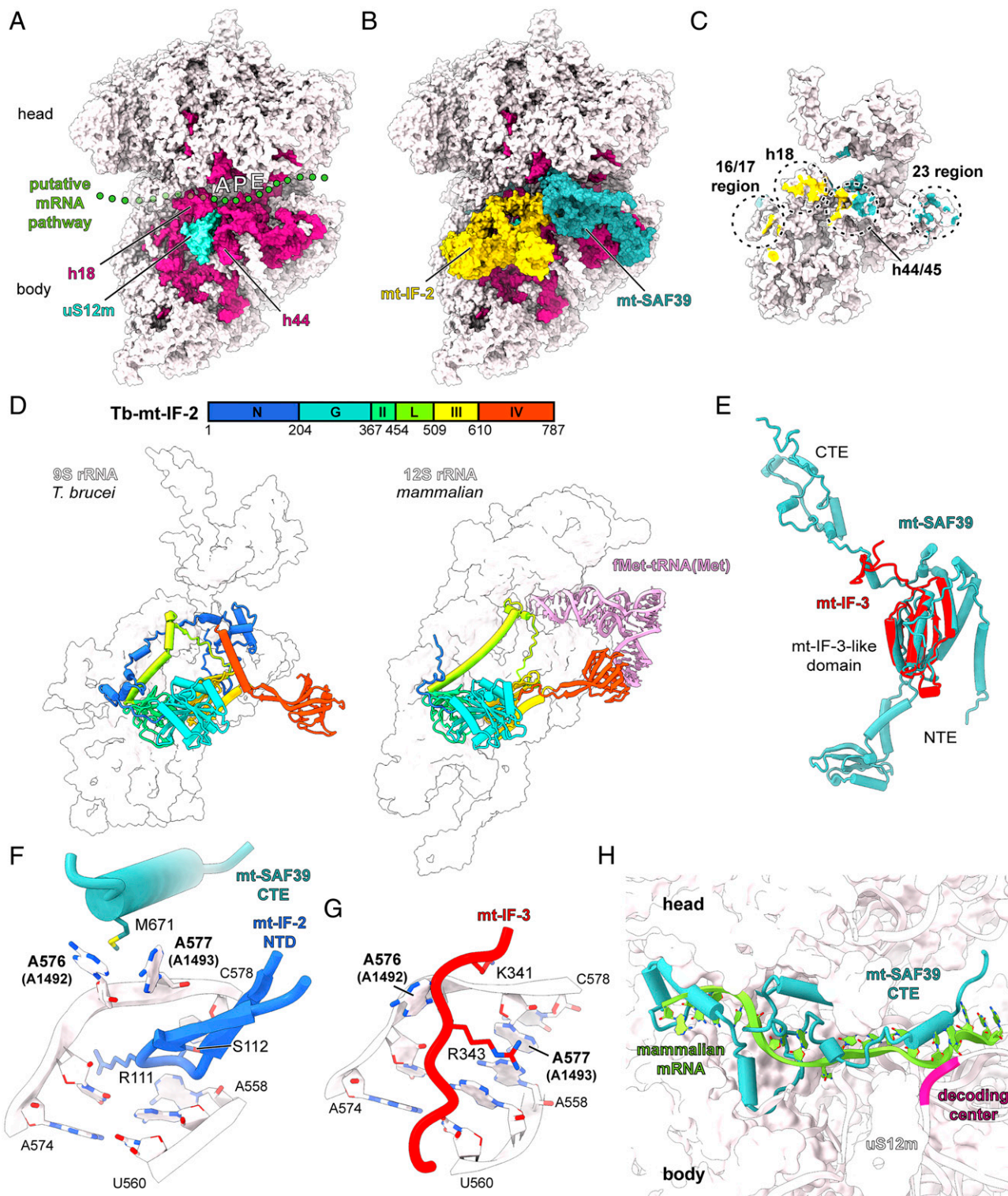


**Fig. 5.** Interactions of mt-IF-2 and mt-IF-3-like assembly factor mt-SAF39 with the decoding center. (A) The putative mRNA path (indicated by green spheres) in the late assembly intermediate, stripped of all assembly factors from the intersubunit interface. (B) Interaction of the mt-IF-2 and mt-SAF39 with the late assembly intermediate 9S rRNA and ribosomal proteins. (C) Interaction sites of mt-IF-2 (yellow) and mt-SAF39 (teal) with the 9S rRNA at a distance up to 3.5 Å. (D) *T. brucei* mt-IF-2 (Left) and mammalian ternary complex [Right, fMet-tRNA(Met) in pink] displayed together with their respective rRNAs. *T. brucei* mt-IF-2 domains and mammalian mt-IF-2 are shown in cartoon and color-coded according to the schematic representation on Top and as defined in ref. 12, respectively. (E) Superposition of mt-IF-3 and mt-IF-3-like assembly factor mt-SAF39. (F) In the late assembly intermediate, the NTD of mt-IF-2 specifically interacts with the decoding center via amino acid residues Arg111 and Ser112. Met671 from the mt-SAF39 CTE additionally stabilizes the flipped decoding center nucleotides A576 and A577 (equivalent to prokaryotic residues A1492 and A1493). All amino acids that are involved in the interactions are depicted as sticks; 9S rRNA backbone is shown as white cartoon with bases as sticks. (G) Interaction of mt-IF-3 with the *T. brucei* mature mt-SSU 9S rRNA. Lys341 and Arg343 are shown as sticks. The corresponding regions of 9S rRNA are shown as in G. (H) The mt-SAF39 CTE protrudes along the mRNA channel, thereby blocking mRNA binding. The mRNA is modeled by superposition of the mammalian mitochondrial translation initiation complex (12) onto *T. brucei* mt-IF-2. Ribosomal proteins are shown as white surfaces and the 9S rRNA as white cartoon. Decoding center nucleotides A576 and A577 and uS12m are highlighted.

These results show that during mt-SSU maturation the NTD domain of mt-IF-2 together with mt-IF-3-like mt-SAF39 specifically interacts with the decoding region to monitor its proper conformation, suggesting a noncanonical role of mt-IF-2.

**Mitochondrial Initiation Factor Does Not Function as a Typical mt-SAF.** To test whether mt-IF-2 plays a double role in translation initiation and mt-SSU assembly, we assumed that its knockdown would lead to an incorrectly assembled mt-SSU and consequently to a decrease of 9S rRNA steady-state levels, as observed before (31, 33, this study). Knockdown of mt-IF-2 leads to a growth retardation (49) and a minor but selective decrease of the 9S rRNA of ~30% when compared to the 12S rRNA (Fig. 6A). This phenotype is qualitatively identical to what was observed after ablation of the previously characterized assembly factors, although less pronounced. This supports our structural findings and indicates that mt-IF-2 plays a role during assembly of the mitoribosomal SSU.

To dissect the mt-IF-2 function in the assembly intermediates in more detail, we generated two cell lines based on the above-described mt-IF-2 RNAi cell line that allowed for inducible down-regulation of mt-IF-2, while simultaneously expressing either the full-length (FL-IF-2) protein or an N-terminally truncated version ( $\Delta$ N-IF-2) using tetracycline (tet) induction from an ectopic locus. The  $\Delta$ N-IF-2 version is truncated at Thr167 and is therefore lacking the N-terminal domain, which interacts with the decoding center in our structures (Fig. 5F). The efficiency of the RNAi-mediated down-regulation of mt-IF-2 in the parent cell line is  $\geq 90\%$ , as gauged by Western blot analysis (Fig. 6B). FL-IF-2 and the  $\Delta$ N-IF-2 version are roughly 5 $\times$  overexpressed (Fig. 6B), and, as evident from the growth curve, the reexpression of the ectopic FL-IF-2 fully complements the RNAi-mediated depletion of endogenous mt-IF-2 (Fig. 6C), while the  $\Delta$ N-IF-2 is not able to complement the growth retardation and shows a 20% decrease in 9S rRNA steady-state levels (Fig. 6D). These biochemical results are consistent with our observation that the mt-IF-2 N-terminal domain plays a role in mt-SSU assembly. Since N-terminal truncation of mt-IF-2 has a lesser effect on 9S rRNA stability than observed for deletions of other assembly factors in this system, we conclude that mt-IF-2 serves as a nonessential final quality-control check of the decoding center at late stage of maturation.

## Discussion

Compared to bacterial and eukaryotic cytosolic ribosome assembly, relatively little is known about ribosome assembly in mitochondria. There is increasing evidence that the mitoribosome maturation process involves a large number of assembly factors, which bridge the gap between the import of the mitoribosomal proteins to the mitochondria and their successive association with the mitochondrial rRNA. For the small mitoribosomal subunit, only recently the atomic description of the mt-SSU assembly provided first structural insights into the assembly process in *T. brucei* (31). At that time, two other mt-SSU-like complexes from this study, referred to as middle and late assembly intermediates, were resolved at a lower resolution and indicated a probable assembly pathway. Here, we provide the reconstructions of these assembly intermediates at near-atomic resolution. We identified five previously undescribed mt-SAFs, the ablation of which proved detrimental for cell growth and 9S rRNA stability, and mt-IF-2 at the intersubunit interface. We revealed how mt-IF-3-like mt-SAF39 CTE and mt-IF-2 NTD monitor the maturation of the functionally important regions of the mt-SSU by specifically interacting with the decoding center. We also showed that the absence of mt-IF-2 NTD affects the 9S rRNA stability as observed for other assembly factors, although to a lesser extent. Furthermore, from the structure it becomes evident how

mt-SAF39 CTE prevents mRNA recruitment by occupying the mRNA channel of the mt-SSU.

This study, together with the structure of the previously published mt-SSU assembly intermediate and the mature trypanosomal mt-SSU, conveys detailed mechanistic description of the individual assembly steps (Fig. 7). In addition to association of several mitoribosomal proteins and conformational changes of 9S rRNA, distinct modules of assembly factors need to exchange between assembly intermediates. For instance, to allow the head to rotate and adopt a mature conformation, a block of 19 intertwined mt-SSU assembly-specific assembly factors, covering the intersubunit side and forming a wedge between the head and the body, must dissociate. However, in order to prevent the premature exposure of the incomplete mt-SSU intersubunit side, the dissociation of this particular mt-SAF cluster is in the middle assembly intermediate coupled with the association of five additional assembly factors, four mitoribosomal proteins, one of which is uS12m, a ubiquitous structuring unit of the decoding center, and an initiation factor, mt-IF-2. The incorporation of uS12m further indicates that middle and late assembly intermediates represent final stages of the maturation (52). At this stage, mt-IF-2 and mt-IF-3-like mt-SAF39 block mRNA access by binding to the mRNA channel and structurally proofread the integrity and the conformation of the decoding center by interacting with the flipped-out decoding nucleotides A576 and A577 in the 9S rRNA. In the late assembly intermediate, a block of eight mitoribosomal proteins replaces a cluster of 10 mt-SAFs on the solvent-exposed side of the mt-SSU, which results in complete maturation with respect to the mitoribosomal protein content as well as the conformational states of these proteins. Furthermore, once the late assembly intermediate is formed, all 9S rRNA domains are almost completely mature with the exception of helix 44 in the 3' minor domain of the rRNA, which remains shielded by the assembly factors and mt-IF-2. The fact that 5' domain at the solvent-exposed side and the central domain of the 9S rRNA mature prior to 3' domains is consistent with the rRNA domain maturation in prokaryotes (reviewed in ref. 53) and eukaryotes (reviewed in ref. 16), demonstrating common principles of ribosome assembly. In order for the intersubunit side to become available for interactions that must occur during translation, all remaining assembly factors have to dissociate.

The participation of an initiation factor during the mitoribosomal assembly is not entirely surprising, as it was proposed before that initiation factors may play a role beyond translation initiation (23). During cold adaptation, for example, bacterial IF-2 displays a GTPase-associated chaperone activity that could aid in ribosome assembly. The study demonstrated that the longer form of IF-2, i.e., IF-2 $\alpha$ , elicits a more efficient chaperone activity in comparison to the IF-2 $\beta$ , the shorter IF-2 form lacking 158 N-terminal residues, highlighting the important functional difference between these two naturally occurring isoforms. In addition, initiation factor-like assembly factors have also been reported to assist in late-stage maturation of cytosolic small ribosomal subunits (45, 48). In particular, yeast protein Tsr1 that consists of an eIF5B GTPase-like fold, but lacks the residues to bind and hydrolyze GTP, monitors the proper formation of the decoding center in 40S during final stages of maturation. Another important checkpoint of assembly that has been suggested for yeast cytosolic ribosomes is the formation of 80S-like particles (54–56) where association of pre-40S subunit with 60S subunit is promoted by initiation factor eIF5B and leads to a “translation-like” cycle. Such a quality-control step has not been described for bacterial ribosomes so far. In bacteria, binding of several assembly factors overlaps with the binding sites of translation initiation factors in a way that readily prevents translation initiation by immature subunits (57). It is predicted that RbfA, an abundant assembly factor, senses the stability of interactions



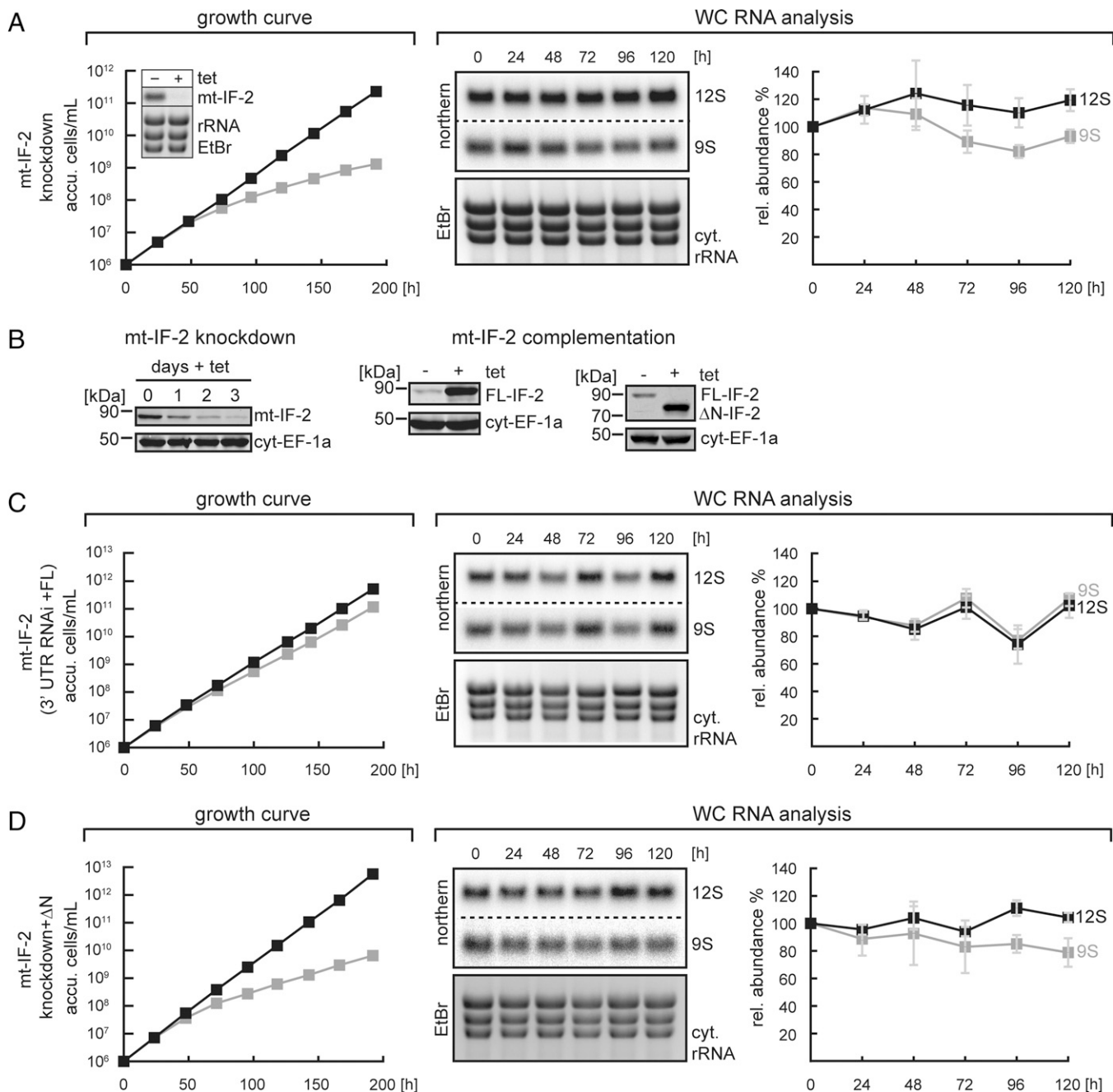


**Fig. 6.** The N-terminal domain IV of mt-IF-2 is essential for cell growth and 9S rRNA stability. (A) Tet-dependent, RNAi-mediated gene knockdown of mt-IF-2 causes growth retardation ~48 h postinduction as shown in the growth curve (black squares, no tet; gray squares, plus tet). The *Inset* shows the corresponding mRNA Northern blot and the cytosolic rRNA stained by EtBr as loading control. (B and C) The knockdown efficiency of mt-IF-2 was determined to be ≥90%, as determined by Western blotting using anti-mt-IF-2 antiserum, with cytosolic elongation factor 1-alpha (cyt-EF-1a) serving as loading control. The EtBr-stained cyt rRNAs are shown as loading control. All cultures were grown in triplicates. In A, C, and D, error bars indicate the average deviation from the mean.

around the 30S decoding center, which is the last region in the SSU particle to mature (58, 59). RbfA therefore controls the stage between ribosome maturation and translation initiation and is displaced directly by IF-3 (59). Analogous to the interplay of RbfA and IF-3 in bacteria, during maturation of trypanosomal mitoribosomes mt-IF-3-like mt-SAF39 may ensure the proper folding of the decoding center, and only when it is completely folded mt-IF-3 replaces mt-SAF39 for translation initiation.

In conclusion, the structural insights combined with biochemical experiments presented here provide evidence for an

alternative, noncanonical role of mt-IF-2, conveyed by its NTD, in the mitoribosomal assembly process that is different from the canonical translation initiation context. It is yet unclear, however, whether mt-IF-2 NTD takes part in assembly of ribosomes in other species or whether this role is trypanosome specific. While not exhibiting high sequence similarity to kinetoplastid mt-IF-2, the mammalian NTD sequence is highly conserved, suggesting that this region is also functionally important in mammals, although it does not play an apparent role during initiation (12).

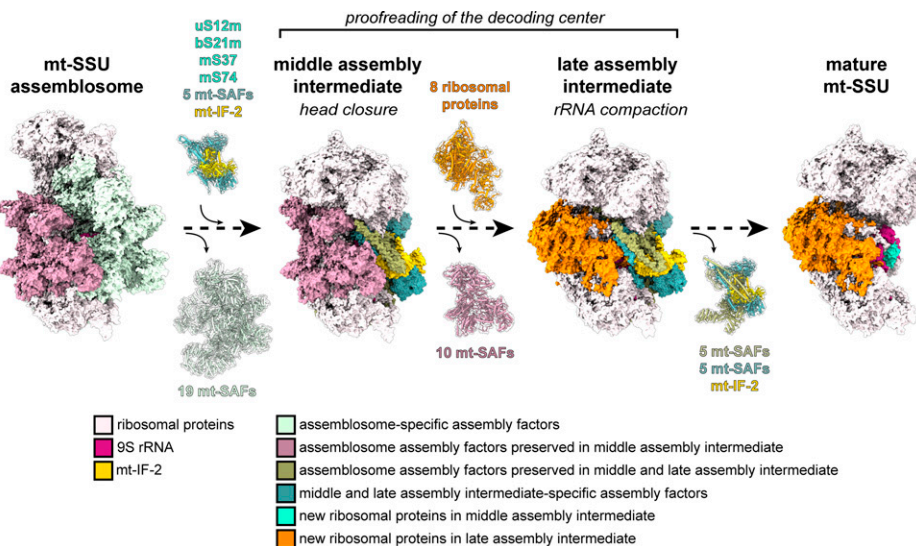


**Fig. 7.** The assembly process of the *T. brucei* mitochondrial SSU is modular. The mt-SSU assemblosome, middle and late assembly intermediates, as well as the mature mt-SSU structures are shown in side views, arranged in the most likely sequence of assembly progression based on their structural features, with landmarks labeled. Distinct modules joining or leaving between different assembly steps are shown in isolation and are colored according to the indicated scheme.

## Materials and Methods

**Cell Culture.** *T. brucei* cell strain 427 (60) and its RNAi-competent derivative BS19.3 (31, 33) were grown as described in [SI Appendix](#).

**Transgenic Cell Lines.** *T. brucei* strain 427 (60) was used as the parental cell line for C-terminal in situ tagging of mitoribosomal LSU protein mL78 (Tb927.10.11050) and uS17m (Tb927.9.11300) with the PTP-tandem affinity tag containing protein A and protein C epitopes separated by a TEV cleavage site (61) as described previously (7, 31). The 427-derived RNAi-competent cell line BS19-3 (31, 33) was used to generate the mt-SAF35-39 and mt-IF-2 knock-down cell lines. Transfection and clonal selection was performed as described in [SI Appendix](#).

**Growth Curves.** *T. brucei* RNAi or complementation cell lines were set to a density of  $1 \times 10^6$  cells/mL in total 6 mL SDM79 (62). The culture was split, and one flask was induced with  $1 \mu\text{g/mL}$  tet. Cells were counted approximately every 24 h, and cultures were diluted to  $1 \times 10^6$  cells/mL accordingly.

**Preparation of Mitochondrial Vesicles.** Preparation of mitochondrial vesicles from large-scale cultures was performed according to ref. 7 and is described in detail in ref. 63. Briefly, up to  $1 \times 10^{12}$  cells (density maximally at  $6 \times 10^7$  cells/mL) were harvested by centrifugation, washed with  $1 \times$  SBG (20 mM sodium phosphate, pH 7.9; 20 mM glucose; 0.15 M NaCl) and lysed by nitrogen cavitation (70 bar, 45 to 60 min) at isotonic conditions using  $1 \times$  SoTE (600 mM sorbitol, 20 mM Tris-HCl pH 7.5, 1 mM ethylenediaminetetraacetic acid). The lysate was subjected to differential centrifugation and subsequent DNase digestion as detailed in ref. 63. The mitochondrial vesicles were further purified using density gradient centrifugation in a 18/21/25/28% (wt/vol) Nycodenz step-gradient containing  $1 \times$  SoTE. The homogenous vesicle population at the interface of the 21% and 25% (wt/vol) Nycodenz layer was harvested, washed with  $1 \times$  SoTE to eliminate residual Nycodenz, resuspended in  $1 \times$  SoTE, flash frozen in liquid nitrogen, and subsequently stored at  $-80^\circ\text{C}$ .

**Western Blot and Antibodies.** To verify mt-IF-2 knockdown and complementation, whole cell lysate ( $\sim 1 \times 10^6$  cells/lane) was separated using sodium dodecyl sulfate–polyacrylamide gel electrophoresis, transferred to nitrocellulose membranes, and probed with the following antibodies: antimitochondrial initiation factor 2 (mIF2) (dilution 1:500); antielongation factor 1a (EF1a) (dilution 1:20,000, Merck Millipore). The blots were subsequently visualized

with a Li-Cor Odyssey CLx infrared imaging system using the goat anti-mouse 680LT purchased from Li-Cor Biosciences as secondary antibody (dilution of 1:20,000). All antibody dilutions were done in  $1 \times$  phosphate-buffered saline containing 3% (wt/vol) milk powder and 0.1% (vol/vol) Tween 20.

**Northern Blot of Mitochondrial rRNA Steady States.** Detailed protocols for Northern analysis of mitochondrial 9S and 12S rRNA steady-state levels can be found in [SI Appendix](#).

**Cryo-EM Sample Preparation, Data Acquisition, and Processing.** The reprocessing of the available cryo-EM datasets of purified PTP-tagged small (uS17m-PTP; Tb927.9.11300) and large subunit (mL78-PTP; Tb927.10.11050) mitoribosomal particles that were acquired previously (7, 31) and described in detail in [SI Appendix](#).

**Model Building, Refinement, and Interpretation.** Details of the model building, refinement, and interpretation can be found in [SI Appendix](#).

**Creation of Figures.** Figures of cryo-EM densities and molecular models were generated using University of California San Francisco (UCSF) Chimera (64), UCSF ChimeraX (65), and the PyMOL Molecular Graphics System, version 2.0 Schrödinger, LLC.

**Data Availability.** All study data are included in the article and/or supporting information. Coordinates and maps data have been deposited in the Protein Data Bank (PDB): 7PUA (66) and 7PUB (67), and in the Zenodo databank (<https://zenodo.org/record/5833372#YdwTAi8w1Ok>): middle\_postprocess\_masked.mrc (68) and late\_postprocess\_masked.mrc (68).

**ACKNOWLEDGMENTS.** We thank Bernd Schimanski for the BS19.3 “single marker WT427” cell line and the ETH Zurich Scientific Centre for optical and electron microscopy (ScopeM) for access to electron microscopy equipment. T.L. also thanks M. Jaskolowski, A. Jomaa, S. Mattei, and E. Kummer for support and useful advice. We acknowledge EMBO long-term fellowship (1074-2019) (awarded to T.L.). This work was funded by the Swiss National Science Foundation (SNSF) (Grant 31003A\_182341), the National Center of Excellence in RNA and Disease of the SNSF (project funding 182880), and in part by the Roessler Prize, Ernst Jung Prize, and Otto Naegeli Prize for Medical Research, as well as by ETH Research Grant ETH-40 16-2 (to N.B.).

1. T. M. Schmeing, V. Ramakrishnan, What recent ribosome structures have revealed about the mechanism of translation. *Nature* **461**, 1234–1242 (2009).
2. T. W. O'Brien, The general occurrence of 55 S ribosomes in mammalian liver mitochondria. *J. Biol. Chem.* **246**, 3409–3417 (1971).
3. N. Tiller, R. Bock, The translational apparatus of plastids and its role in plant development. *Mol. Plant* **7**, 1105–1120 (2014).

4. A. Amunts, A. Brown, J. Toots, S. H. W. Scheres, V. Ramakrishnan, Ribosome. The structure of the human mitochondrial ribosome. *Science* **348**, 95–98 (2015).
5. B. J. Greber *et al.*, Ribosome. The complete structure of the 55S mammalian mitochondrial ribosome. *Science* **348**, 303–308 (2015).
6. N. Desai, A. Brown, A. Amunts, V. Ramakrishnan, The structure of the yeast mitochondrial ribosome. *Science* **355**, 528–531 (2017).

7. D. J. F. Ramrath *et al.*, Evolutionary shift toward protein-based architecture in trypanosomal mitochondrial ribosomes. *Science* **362**, eaau7735 (2018).
8. F. Waltz *et al.*, Small is big in *Arabidopsis* mitochondrial ribosome. *Nat. Plants* **5**, 106–117 (2019).
9. M. Liu, L. Spremulli, Interaction of mammalian mitochondrial ribosomes with the inner membrane. *J. Biol. Chem.* **275**, 29400–29406 (2000).
10. S. Pfeffer, M. W. Woellhaf, J. M. Herrmann, F. Förster, Organization of the mitochondrial translation machinery studied in situ by cryoelectron tomography. *Nat. Commun.* **6**, 6019 (2015).
11. B. J. Greber *et al.*, Architecture of the large subunit of the mammalian mitochondrial ribosome. *Nature* **505**, 515–519 (2014).
12. E. Kummer *et al.*, Unique features of mammalian mitochondrial translation initiation revealed by cryo-EM. *Nature* **560**, 263–267 (2018).
13. Y. Itoh *et al.*, Mechanism of membrane-tethered mitochondrial protein synthesis. *Science* **371**, 846–849 (2021).
14. D. Kressler, E. Hurt, J. Bäbler, A puzzle of life: Crafting ribosomal subunits. *Trends Biochem. Sci.* **42**, 640–654 (2017).
15. Z. Shajani, M. T. Sykes, J. R. Williamson, Assembly of bacterial ribosomes. *Annu. Rev. Biochem.* **80**, 501–526 (2011).
16. S. Klinge, J. L. Woolford Jr., Ribosome assembly coming into focus. *Nat. Rev. Mol. Cell Biol.* **20**, 116–131 (2019).
17. J. Bäbler, E. Hurt, Eukaryotic ribosome assembly. *Annu. Rev. Biochem.* **88**, 281–306 (2019).
18. P. Traub, M. Nomura, Structure and function of *E. coli* ribosomes. V. Reconstitution of functionally active 30S ribosomal particles from RNA and proteins. *Proc. Natl. Acad. Sci. U.S.A.* **59**, 777–784 (1968).
19. K. H. Nierhaus, The assembly of prokaryotic ribosomes. *Biochimie* **73**, 739–755 (1991).
20. C. Peña, E. Hurt, V. G. Panse, Eukaryotic ribosome assembly, transport and quality control. *Nat. Struct. Mol. Biol.* **24**, 689–699 (2017).
21. J. L. Woolford Jr., S. J. Baserga, Ribosome biogenesis in the yeast *Saccharomyces cerevisiae*. *Genetics* **195**, 643–681 (2013).
22. K. Karbstein, Quality control mechanisms during ribosome maturation. *Trends Cell Biol.* **23**, 242–250 (2013).
23. A. Brandt *et al.*, Translation initiation factor IF2 contributes to ribosome assembly and maturation during cold adaptation. *Nucleic Acids Res.* **47**, 4652–4662 (2019).
24. D. De Silva, Y. T. Tu, A. Amunts, F. Fontanesi, A. Barrientos, Mitochondrial ribosome assembly in health and disease. *Cell Cycle* **14**, 2226–2250 (2015).
25. D. F. Bogenhagen, D. W. Martin, A. Koller, Initial steps in RNA processing and ribosome assembly occur at mitochondrial DNA nucleoids. *Cell Metab.* **19**, 618–629 (2014).
26. A. A. Jourdain, E. Boehm, K. Maundrell, J.-C. Martinou, Mitochondrial RNA granules: Compartmentalizing mitochondrial gene expression. *J. Cell Biol.* **212**, 611–614 (2016).
27. M. Emdadul Haque, D. Grasso, C. Miller, L. L. Spremulli, A. Saada, The effect of mutated mitochondrial ribosomal proteins S16 and S22 on the assembly of the small and large ribosomal subunits in human mitochondria. *Mitochondrion* **8**, 254–261 (2008).
28. X. Pérez-Martínez *et al.*, Protein synthesis and assembly in mitochondrial disorders. *Curr. Top. Med. Chem.* **8**, 1335–1350 (2008).
29. A. Rötig, Human diseases with impaired mitochondrial protein synthesis. *Biochim. Biophys. Acta* **1807**, 1198–1205 (2011).
30. O. Feron, Pyruvate into lactate and back: From the Warburg effect to symbiotic energy fuel exchange in cancer cells. *Radiother. Oncol.* **92**, 329–333 (2009).
31. M. Saurer *et al.*, Mitoribosomal small subunit biogenesis in trypanosomes involves an extensive assembly machinery. *Science* **365**, 1144–1149 (2019).
32. H. Soufari *et al.*, Structure of the mature kinetoplastid mitoribosome and insights into its large subunit biogenesis. *Proc. Natl. Acad. Sci. U.S.A.* **117**, 29851–29861 (2020).
33. M. Jaskolowski *et al.*, Structural insights into the mechanism of mitoribosomal large subunit biogenesis. *Mol. Cell* **79**, 629–644.e4 (2020).
34. V. Tobiasson *et al.*, Interconnected assembly factors regulate the biogenesis of mitoribosomal large subunit. *EMBO J.* **40**, e106292 (2021).
35. A. Brown *et al.*, Structures of the human mitochondrial ribosome in native states of assembly. *Nat. Struct. Mol. Biol.* **24**, 866–869 (2017).
36. T. Lenarčič *et al.*, Stepwise maturation of the peptidyl transferase region of human mitoribosomes. *Nat. Commun.* **12**, 3671 (2021).
37. M. Cipullo, G. V. Gesé, A. Khawaja, B. M. Hällberg, J. Rorbach, Structural basis for late maturation steps of the human mitoribosomal large subunit. *Nat. Commun.* **12**, 3673 (2021).
38. H. S. Hillen *et al.*, Structural basis of GTPase-mediated mitochondrial ribosome biogenesis and recycling. *Nat. Commun.* **12**, 3672 (2021).
39. V. Chandrasekaran *et al.*, Visualising formation of the ribosomal active site in mitochondria. *eLife* **10**, e68806 (2021).
40. J. Cheng, O. Berninghausen, R. Beckmann, A distinct assembly pathway of the human 39S late pre-mitoribosome. *Nat. Commun.* **12**, 4544 (2021).
41. R. Rudler *et al.*, Identification of a new cryptochrome class. Structure, function, and evolution. *Mol. Cell* **11**, 59–67 (2003).
42. C. Oefner, H. Schulz, A. D'Arcy, G. E. Dale, Mapping the active site of *Escherichia coli* malonyl-CoA-acyl carrier protein transacylase (FabD) by protein crystallography. *Acta Crystallogr. D Biol. Crystallogr.* **62**, 613–618 (2006).
43. S. C. Dillon, A. Bateman, The Hotdog fold: Wrapping up a superfamily of thioesterases and dehydratases. *BMC Bioinformatics* **5**, 109 (2004).
44. L. S. Pidugu, K. Maity, K. Ramaswamy, N. Suroliya, K. Suguna, Analysis of proteins with the 'hot dog' fold: Prediction of function and identification of catalytic residues of hypothetical proteins. *BMC Struct. Biol.* **9**, 37 (2009).
45. A. Heuer *et al.*, Cryo-EM structure of a late pre-40S ribosomal subunit from *Saccharomyces cerevisiae*. *eLife* **6**, e30189 (2017).
46. A. Razi, A. Guarné, J. Ortega, The cryo-EM structure of YjeQ bound to the 30S subunit suggests a fidelity checkpoint function for this protein in ribosome assembly. *Proc. Natl. Acad. Sci. U.S.A.* **114**, E3396–E3403 (2017).
47. A. Razi *et al.*, Role of Era in assembly and homeostasis of the ribosomal small subunit. *Nucleic Acids Res.* **47**, 8301–8317 (2019).
48. A. Scaiola *et al.*, Structure of a eukaryotic cytoplasmic pre-40S ribosomal subunit. *EMBO J.* **37**, e98499 (2018).
49. F. Charrière, T. H. Tan, A. Schneider, Mitochondrial initiation factor 2 of *Trypanosoma brucei* binds imported formylated elongator-type tRNA(Met). *J. Biol. Chem.* **280**, 15659–15665 (2005).
50. T. H. Tan, N. Bochud-Allemann, E. K. Horn, A. Schneider, Eukaryotic-type elongator tRNA<sup>Met</sup> of *Trypanosoma brucei* becomes formylated after import into mitochondria. *Proc. Natl. Acad. Sci. U.S.A.* **99**, 1152–1157 (2002).
51. A. P. Carter *et al.*, Crystal structure of an initiation factor bound to the 30S ribosomal subunit. *Science* **291**, 498–501 (2001).
52. S. Mizushima, M. Nomura, Assembly mapping of 30S ribosomal proteins from *E. coli*. *Nature* **226**, 1214 (1970).
53. J. H. Davis, J. R. Williamson, Structure and dynamics of bacterial ribosome biogenesis. *Philos. Trans. R. Soc. Lond. B Biol. Sci.* **372**, 20160181 (2017).
54. S. Lebaron *et al.*, Proofreading of pre-40S ribosome maturation by a translation initiation factor and 60S subunits. *Nat. Struct. Mol. Biol.* **19**, 744–753 (2012).
55. B. S. Strunk, M. N. Novak, C. L. Young, K. Karbstein, A translation-like cycle is a quality control checkpoint for maturing 40S ribosome subunits. *Cell* **150**, 111–121 (2012).
56. H. Ghalei *et al.*, The ATPase Fap7 tests the ability to carry out translocation-like conformational changes and releases Dim1 during 40S ribosome maturation. *Mol. Cell* **68**, 1155 (2017).
57. P. P. Datta *et al.*, Structural aspects of RbfA action during small ribosomal subunit assembly. *Mol. Cell* **28**, 434–445 (2007).
58. A. Schedlbauer *et al.*, A conserved rRNA switch is central to decoding site maturation on the small ribosomal subunit. *Sci. Adv.* **7**, eabf7547 (2021).
59. I. M. Sharma, S. A. Woodson, RbfA and IF3 couple ribosome biogenesis and translation initiation to increase stress tolerance. *Nucleic Acids Res.* **48**, 359–372 (2020).
60. G. A. Cross, Identification, purification and properties of clone-specific glycoprotein antigens constituting the surface coat of *Trypanosoma brucei*. *Parasitology* **71**, 393–417 (1975).
61. B. Schimanski, T. N. Nguyen, A. Günzl, Highly efficient tandem affinity purification of trypanosome protein complexes based on a novel epitope combination. *Eukaryot. Cell* **4**, 1942–1950 (2005).
62. R. Brun, M. Schönenberger, Cultivation and in vitro cloning or procyclic culture forms of *Trypanosoma brucei* in a semi-defined medium. Short communication. *Acta Trop.* **36**, 289–292 (1979).
63. M. Niemann, A. Schneider, A scalable purification method for mitochondria from *Trypanosoma brucei*. *Methods Mol. Biol.* **2116**, 611–626 (2020).
64. E. F. Pettersen *et al.*, UCSF Chimera—A visualization system for exploratory research and analysis. *J. Comput. Chem.* **25**, 1605–1612 (2004).
65. T. D. Goddard *et al.*, UCSF ChimeraX: Meeting modern challenges in visualization and analysis. *Protein Sci.* **27**, 14–25 (2018).
66. T. Lenarčič, M. Leibundgut, M. Saurer, D. J. Ramrath, T. Flügel, D. Boehringer, N. Ban, Middle assembly intermediate of the *Trypanosoma brucei* mitoribosomal small subunit. Protein Data Bank. <https://www.rcsb.org/structure/7PUA>. Deposited 29 September 2021.
67. T. Lenarčič *et al.*, Late assembly intermediate of the *Trypanosoma brucei* mitoribosomal small subunit. Protein Data Bank. <https://www.rcsb.org/structure/7PUB>. Deposited 29 September 2021.
68. T. Lenarčič, M. Leibundgut, N. Ban, Cryo-EM maps: Mitoribosomal small subunit maturation involves formation of initiation-like complexes. Zenodo. <https://zenodo.org/record/5833372#YdwtAi8w1Ok>. Deposited 10 January 2022.